Published in final edited form as:

Huss, J. C., Späker, O., Gierlinger, N., Merritt, D. J., Miller, B. P., Neinhuis, C., et al. (2018). Temperature-induced self-sealing capability of Banksia follicles. Journal of the Royal Society Interface, 15(143): 20180190. doi:10.1098/rsif.2018.0190.

Temperature-induced self-sealing capability of Banksia follicles

Jessica C. Huss, Oliver Spaeker, Notburga Gierlinger, David J. Merritt, Ben P. Miller, Christoph Neinhuis, Peter Fratzl, Michaela Eder

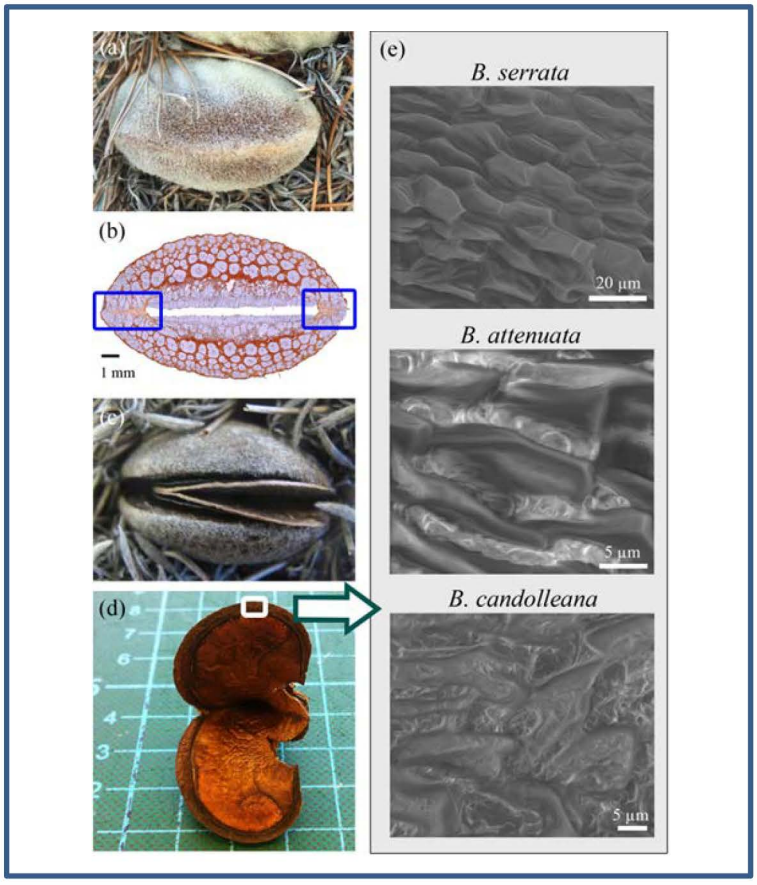

Location and morphology of the junction zone in different Banksia species. (a) Closed single follicle of B. serrata on the woody infructescence. (b) Unstained light microscopy image of a follicle cross-section of B. serrata. Boxes indicate the location of the junction zone. (c) Follicle of B. serrata after opening, still retaining the seeds and a hygroscopic separator plate. (d) Isolated follicle of B. serrata (cuticle and exocarp removed) after drying, showing strongly deformed valves and pronounced lateral crack formation (junction zone lining the valves). Grid: 1x1 cm. (e) Scanning electron microscopy images of the junction zone surface in open follicles of B. serrata, B. attenuata (from Site 3; wax appears bright) and B. candolleana (the sample was cut when the follicle was still hot, showing “smeared” wax features). The box in (d) indicates the regions of (e).

Temperature-induced self-sealing capability of *Banksia* follicles

Jessica C. Huss[1*], Oliver Spaeker[1], Notburga Gierlinger[2], David J. Merritt[3,4], Ben P. Miller[3,4], Christoph Neinhuis[5], Peter Fratzl[1], Michaela Eder[1*]

[1] Max Planck Institute of Colloids and Interfaces, Department of Biomaterials, 14476 Potsdam, Germany
[2] BOKU - University of Natural Resources and Life Sciences, Department of Nanobiotechnology, Institute for Biophysics, 1190 Vienna, Austria.
[3] Kings Park Science, Department of Biodiversity, Conservation and Attractions, Kings Park, WA 6005, Australia
[4] School of Biological Sciences, The University of Western Australia, Crawley, WA 6009, Australia
[5] Technische Universität Dresden, Institute for Botany, 01062 Dresden, Germany

*Corresponding author information: Jessica.Huss@mpikg.mpg.de or Michaela.Eder@mpikg.mpg.de

Abstract

Many plants in fire-prone regions retain their seeds in woody fruits in the plant canopy until the passage of a fire causes the fruit to open and to release the seeds. To enable this function, suitable tissues are required that effectively store and protect seeds until they are released. Here, we show that three different species of the Australian genus *Banksia* incorporate waxes at the interface of the two valves of the follicle enclosing the seeds, which melt between 45-55 °C. Since the melting temperature of the waxes is lower than the opening temperatures of the follicles in all investigated species (*B. candolleana*, *B. serrata*, *B. attenuata*), we propose that melting of these waxes allows the sealing of micro-fissures at the interface of the two valves while they are still closed. Such a self-sealing mechanism likely contributes to the structural integrity of the seed pods, and benefits seed viability and persistence during storage on the plants. Furthermore, we show in a simplified, bio-inspired model system that temperature treatments seal artificially applied surface cuts and restore the barrier properties.

Keywords: self-sealing, bio-inspired materials, fire, *Banksia*, serotiny.

1. Introduction

Biological materials often exhibit multifunctional properties that serve the various needs of the organisms producing them [1]. In harsh environments, specialized structures and mechanisms have evolved to prevent damage or enable efficient recovery from it. Examples of such systems are the fast wound sealing mechanism based on latex coagulation upon injury in fig trees [2], or the pneumatic membrane deformation during wound-sealing in succulent plants, which prevents drought stress in arid regions [3]. In this study, we describe the self-sealing properties of the woody seed pods (follicles) of the Australian plant genus *Banksia*, which result from self-healing of a wax layer. Depending on the species and its distribution range, opening of the follicles (followed by seed release) either occurs at maturity or when exposed to heat or fire, after a delay time of up to 17 years [4-7]. The latter phenomenon is termed 'serotiny' and refers to the time lag between the point of seed maturity and the actual release of the seeds [8]. The follicles of serotinous *Banksia* species have crucial functions in fire-prone ecosystems: they store, protect and finally release viable seeds, and thus – on a larger scale – influence species persistence, the regeneration of populations and the composition of plant communities [9, 10]. The parental plants of some species and populations are killed by fire; therefore, regeneration depends entirely on the successful storage, release and germination of the seeds, followed by the establishment and survival of the seedlings [4, 10, 11]. Since the intervals between bushfires can vary considerably in Australia [12], and fruits are produced and stored over multiple years, the follicles need to have long-term stability and be resistant to biotic and abiotic factors causing disintegration. At the same time, they must maintain their functional capacity to open and release the seeds in response to environmental stimuli. In this work, we present a self-sealing mechanism discovered in follicles of *Banksia attenuata* R.Br., *B. candolleana* Meisn. and *B. serrata* L.f. - species that occur in different geographic regions of Australia and exhibit different levels of intra- and interspecific serotiny [4, 5, 7]. As recently clarified within one species, variations in the degree of serotiny and opening temperatures arise through geometric variations of the follicle valves [13], rather than chemical changes in the sealing agent between the valves [14]. On this basis, we explore a potential self-sealing function of the waxes identified at the interface of the two follicle valves. The principles which underlie temperature induced self-sealing are described based on the response of the follicles to gradually increasing temperatures, followed by a chemical, structural and mechanical analysis of the interface between the two follicle valves enclosing the seeds. The self-sealing capability is then demonstrated for a wood-based model system inspired by the findings for these *Banksia*

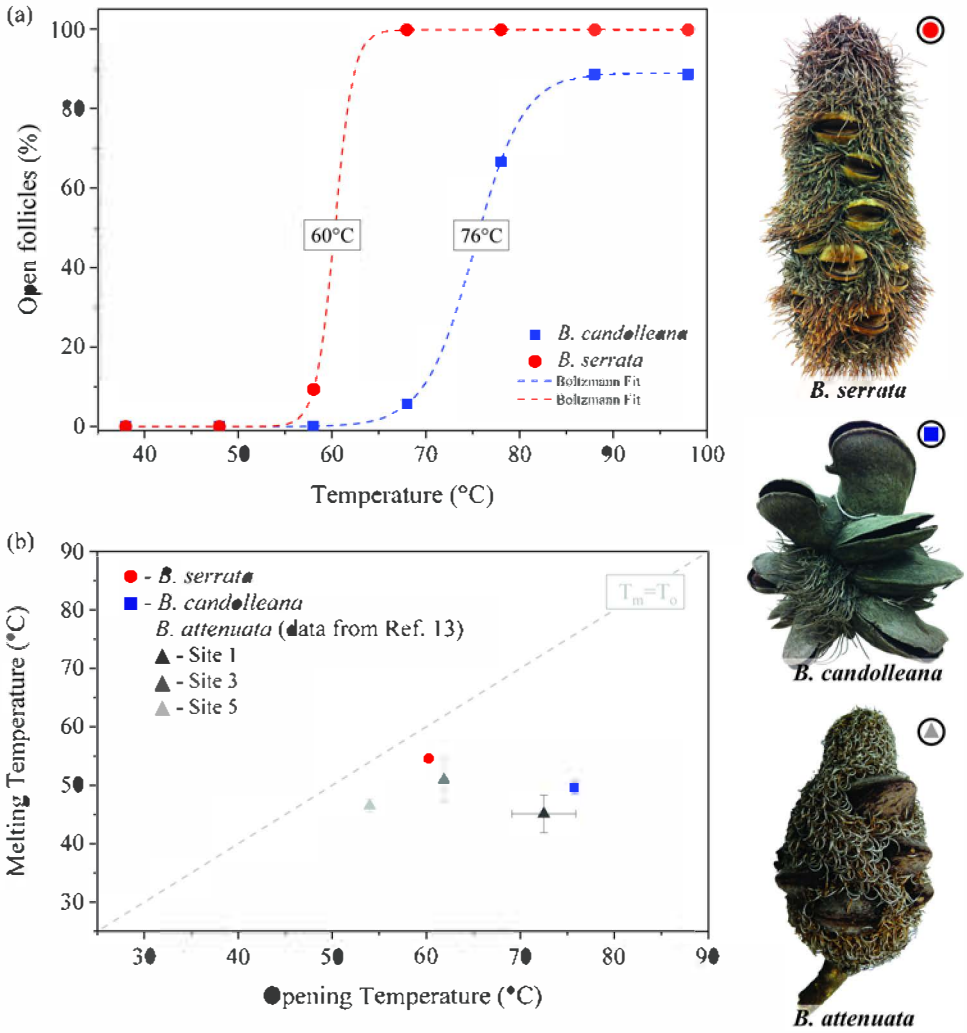

Figure 1. Temperature requirements for follicle opening in three *Banksia* species. (a) share of open follicles during stepwise heating of whole fruit cones of *B. serrata* and *B. candolleana* with initially closed follicles. Highlighted temperatures (boxes) indicate temperatures for 50% open follicles. (b) Wax melting temperatures plotted against follicle opening temperatures for all three *Banksia* species (± SE).

species. Finally, the ecological and technical relevance of such properties are briefly discussed. The classification of follicle tissue, and all terminology used in this study, is based on previous work performed by Wardrop [14] and Huss et al. [13].

2. Materials and methods

2.1 Sample collection and preparation

Banksia serrata infructescences (cones, Fig. 1) were collected from a plant in the Botanical Garden of the University of Bonn (Germany, collected in July 2014) and from the Banksia Farm in Mount Barker (Western Australia, collected in September 2016), whereas *B. attenuata* and *B. candolleana* cones were directly sourced from the field in Western Australia (collection sites of *B. attenuata* along an environmental gradient - Site 1: 29.62080 °S, 115.21177 °E and 29.62343 °S, 115.21430 °E; Site 3: 30.57174 °S, 115.46120 °E; Site 5: 31.69048 °S, 115.87981 °E and 31.68662 °S, 115.88483 °E. *B. candolleana* collected from 30.04438 °S, 115.32618 °E). *Banksia serrata* is naturally distributed along the east coast of Australia, and *B. attenuata* and *B. candolleana* occur within south western Australia. Prior to the opening experiments, mature cones of *B. candolleana* were stored for 18 months (collected in May 2014) and *B. serrata* for 15 months (collected in July 2014) under laboratory conditions (no opening of follicles occurred during storage).

2.2 Determination of the opening temperature

Closed follicles of *B. candolleana* (n=18) and *B. serrata* (n=33) were subjected to gradual heating (temperature increased stepwise +10 °C/ 24 h; starting at 40 °C) with an oven/climatic chamber (VCL 4010, Vötsch). The temperature inside the oven was monitored with a thermocouple (K406-484, TC Direct) and the number of open follicles determined after every heating step (every 24 h). Experimental data for the opening temperature and wax melting temperature of *B. attenuata* was used from Huss et al. [13].

2.3 Scanning Electron microscopy

Micrographs of the junction zone surface of open follicles were taken with an environmental scanning electron microscope (FEI Quanta 600-FEG) at 0.75 Torr sample chamber pressure and an acceleration voltage of 5 – 7.5 keV.

2.4 Confocal Raman microscopy

For acquiring depth scans on water immersed 20 µm thick follicle cross sections of *B. serrata*, a confocal Raman microscope (alpha 300 RA, WITec, Germany), equipped with a 785 nm laser (Xtra-PS, TOPTICA Photonics), was used in combination with a blazed grating (600 g/mm, UHTS spectrometer, WITec) and a deep-depletion CCD camera (DU401A BR-DD, ANDOR). Imaging was performed via a 100 × oil immersion objective (NA 1.4, Zeiss) and an integration time of 2 s.

The determination of the wax melting temperature for *B. serrata* and *B. candolleana* was performed via a confocal Raman microscope (CRM200, WITec) with a diode pumped 785 nm laser (Toptica Photonics), which was dispersed onto the CCD camera (PI-MAX, Princeton Instruments) with a grating of 300 g/mm (Acton spectrograph, Princeton Instruments). Single spectra were recorded by focussing the laser onto the junction zone through a 20 × air objective (NA 0.4, Nikon). The water immersed tissue sections were heated with an external stage (FTIR-600, Linkam) to temperatures from 25-60 °C and spectra acquired with 5 s integration time after holding the temperature constant for 2 min. During the process of heating and spectral acquisition, the microscope objective was heated to the same temperature as the sample via a heating collar (OBJ COLLAR, okolab) in combination with a temperature controller (UNO, okolab) to prevent condensation on the lens at higher temperatures. After background removal, the intensity ratio $I_{2885cm}^{-1}/I_{2880cm}^{-1}$ was calculated for each spectrum (as suggested by Lewis and McElhaney [15]) and the dataset then fitted with a concatenated Boltzmann Fit (Fig. S1) in OriginPro (version 9.1, OriginLab). The inflection point of the fitted curve was used for comparison of the species and their respective opening temperature (values for opening temperature reflect those at which 50% of the follicles opened).

The same instrument was used for imaging of the junction zone by using a piezo-scanner (P-500, Physik Instrumente) and a 50 × objective (NA 0.65 IR, Olympus LC Plan N). The sections of *B. serrata* (20 µm) were scanned with an integration time of 2 s before and after boiling them in water for 5 min on an external heating stage. Simple sum filters were applied in WiTec Project FOUR Plus for generating intensity maps of different regions in the junction zone. The image scans of all species were analysed with the cluster analysis tool with 3 clusters and another 3 sub-clusters of the identified wax cluster (Fig. S2). The sub-cluster spectrum with the clearest wax features was then selected for comparison after background and cosmic ray removal. Overview images of the sample were obtained before and after

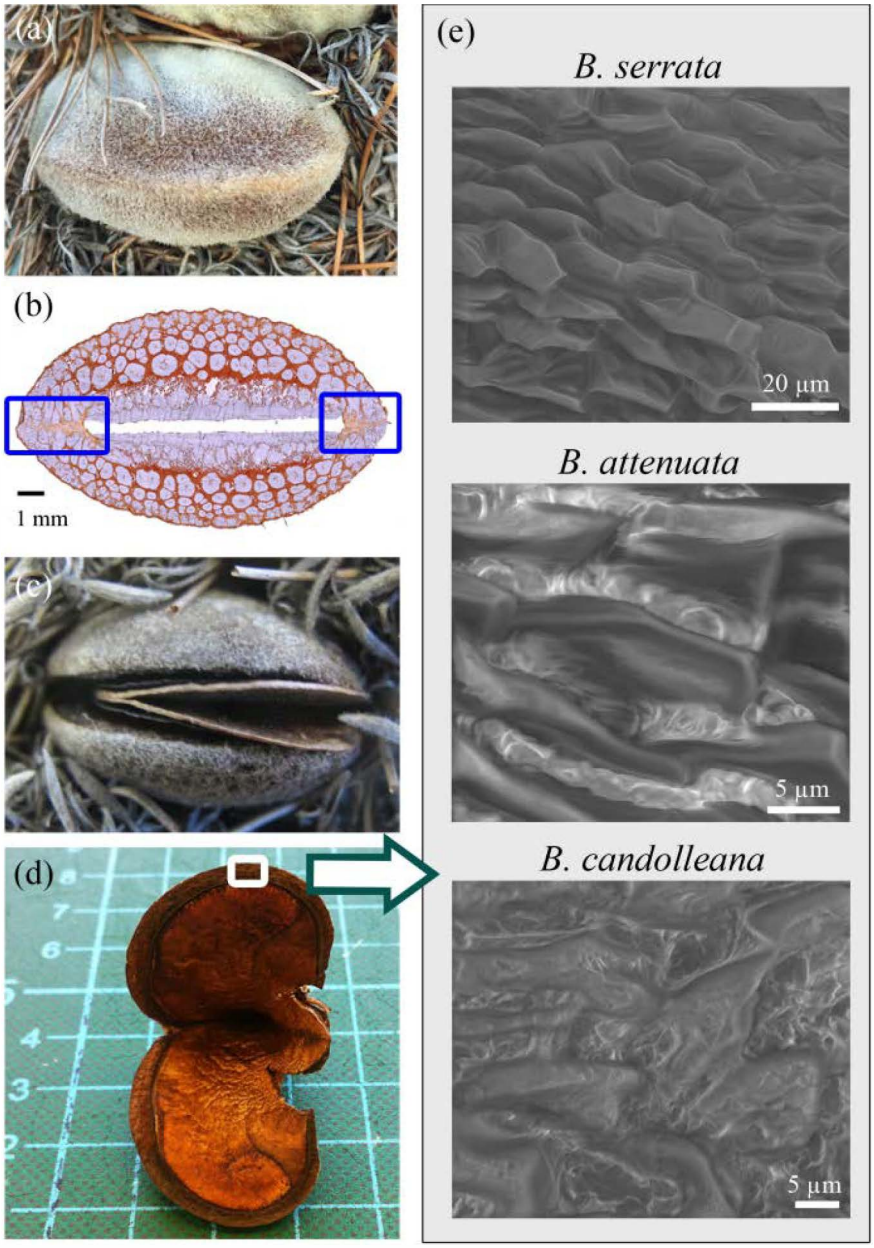

Figure 2. Location and morphology of the junction zone in different *Banksia* species. (a) Closed single follicle of *B. serrata* on the woody infructescence. (b) Unstained light microscopy image of a follicle cross-section of *B. serrata.* Boxes indicate the location of the junction zone. (c) Follicle of *B. serrata* after opening, still retaining the seeds and a hygroscopic separator plate. (d) Isolated follicle of *B. serrata* (cuticle and exocarp removed) after drying, showing strongly deformed valves and pronounced lateral crack formation (junction zone lining the valves). Grid: 1x1 cm. (e) Scanning electron microscopy images of the junction zone surface in open follicles of *B. serrata*, *B. attenuata* (from Site 3; wax appears bright) and *B. candolleana* (the sample was cut when the follicle was still hot, showing "smeared" wax features). The box in (d) indicates the regions of (e).

boiling by using the 3D stitching mode of a digital microscope (VHX S550E, Keyence) at 700 × magnification (VH-Z100UR lens, Keyence).

2.5 Temperature controlled tensile tests of the junction zone

For the tensile testing of the junction zone (Fig. S3), single follicles of *B. attenuata* were isolated with a hand saw (H-150 blade, Z Hanbai), followed by applying 1.5 – 2 mm broad pre-cuts perpendicular to the junction zone using an Ever-Sharp-Blade (Apollo Herkenrath). These pre-cuts were then isolated with the hand saw by cutting out samples tangentially to the follicle tip including parts of the underlying mesocarp, which was used to glue each sample on the end parts of two trimmed oak veneer holders (55 × 7 × 0.5 mm). Only specimens with glue (Uhu Holz Max, Uhu) attached at the two ends of the samples were selected for testing (no glue bridging the two holders or spreading into the JZ). Testing specimens ($n_{Site\ 1} = 48$, $n_{Site\ 5} = 52$) were stored for at least 24 h in order to allow the glue to harden.

Tensile tests were performed with a Zwicki-Linie Z 2,5 (Zwick) machine with a 1 kN load cell (XforceHP, Zwick) and two stainless steel 1 kN chuck jaws (8133, Zwick). The distance between the jaws was set to 80 mm. The sample was fastened at the upper clamp at room temperature and then heated up to the pre-defined temperature (20, 40, 60, 70 or 80 °C) using a 150 W Infrared-Spot (Optron) coupled with a radiation pyrometer (IN810 CF2, Optron) for temperature control. Three minutes after reaching the targeted temperature, the lower jaw was fastened and the tensile test commenced. A preload of 0.02 N was applied and the samples were tested with a test speed of 0.005 mm s^{-1} until failure of the junction zone. The maximum force F_{max} was used for calculating the ultimate tensile stress by normalization with the contact area of the two follicle valves. The contact area of the fractured surface was recorded with a digital microscope (VHX 550E, Keyence) using a 100 × magnification in the reflection mode. Afterwards the area was determined in Adobe Photoshop (CS5, 64 Bit, Adobe Systems).

2.6 Bio-inspired model system

A simple bio-inspired model system was developed to test the previously identified sealing mechanism on a larger scale. To illustrate its applicability with a well characterised and commonly used material, we chose pine wood. The pine wood platelets originated from a 1 m long pine wood strip (oriented along the longitudinal axis of the stem), which was cut into uniform pieces with dimensions of 15 mm in the tangential direction, 27.5 mm in the radial direction and 1.2 mm in the longitudinal direction by using a band saw. All pieces were

immersed into liquid Carnauba wax (No. 1, Sigma-Aldrich) heated on top of a heating plate, T≈100 °C) for 10 min until all air bubbles disappeared. Before placing the samples on an aluminium foil for cooling, they were quickly rotated 180 ° and back again in order to allow even distribution of the liquid wax on the surface. After cooling, six cuts (three parallel to the fibres, three perpendicular to the fibres) of 1-2 mm depth were manually applied by pressing the tip of a scalpel blade (No. 22, Bayha) into the upper surface of each sample. Experimental data for the bio-inspired model system was acquired by placing half of the pine wood platelets (n=8) horizontally in an oven at 115 °C for 15 min. After cooling of the samples, a drop of Fuchsin-Chrysoidin-Astrablue (FCA after Etzold) staining solution prepared as described in Mulisch and Welsch [16] was spread on the whole upper sample surface of all sample platelets (n=16) using a pipette, and then dried with a paper towel after 10-15 s. The solution stains lignified tissue in red and non-lignified tissue in blue, and was used for testing the presence of unsealed areas of wood, which was investigated under a light microscope (M165C, Leica).

3. Results and discussion

3.1 Temperature variations in fruit opening

Variations in the required temperatures for follicle opening exist between the investigated species (Fig. 1a), showing that follicles of *B. candolleana* require a higher temperature for opening than *B. serrata*. These observations seem to reflect their described levels of serotiny: *B. candolleana* is a highly serotinous species, whereas *B. serrata* is a weakly serotinous species [5, 7]. A similar relationship between serotiny levels and the temperatures required for follicle opening has been described in different populations of *B. attenuata* along a climatic gradient, where levels of serotiny [4] and follicle opening temperatures increase [13] as habitats become drier, hotter and more fire-prone. Notably, the opening temperatures of follicles of *B. candolleana* and *B. attenuata* (75 °C and 68-72 °C, respectively) are similar for populations of these two species sourced from similar locations, suggesting that the opening temperatures amongst species might be common, and related to the environmental conditions of their habitat.

The waxes previously identified at the interface of the two valves in the junction zone of *B. attenuata* and the waxes of the newly investigated species all display a narrow temperature range for melting; with a slightly higher phase transition temperature for *B. serrata* (54.5 ± 0.2 °C) when compared to *B. attenuata* and *B. candolleana* (45.1 ± 3.2 °C to 50.9 ± 3.9 °C;

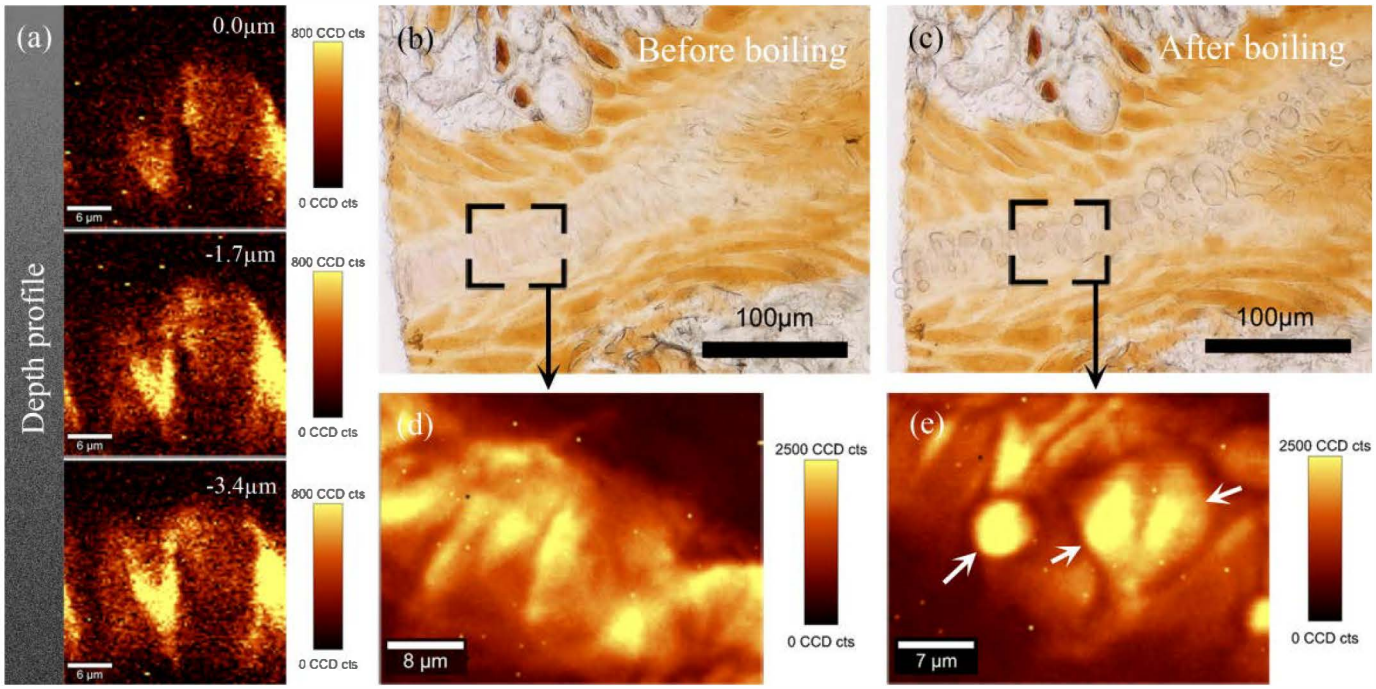

Figure 3. Mapping of the wax in the junction zone of *B. serrata* follicles. (a) Raman images taken at different depths of an area in the junction zone (integration of the spectral region from 1277-1313 cm^{-1}) showing a zig-zag distribution of the wax in between the interdigitating structures (shown in Fig. 2e). (b-c) Digital microscopy images of the junction zone tissue before (non-heated) and after boiling in water. After boiling, small droplets are visible along the junction zone. (d-e) Raman images before and after boiling; showing the typical zig-zag distribution of the wax before boiling and the presence of wax droplets afterwards (arrows in e). Both images are based on integration of the spectral region from 2810-2990 cm^{-1}, and show that the wax in the junction zone is able to flow in the liquid state.

Fig. S1). The temperature range for melting is essentially constant and always lower than the opening temperature of the correspondent follicle ($T_m < T_o$ in Fig. 1b). Since melting occurs in a lower temperature range than follicle opening, it cannot be the key to trigger follicle opening, as was originally proposed by Wardrop for the species *B. ornata*, *B. integrifolia* and *B. marginata* [14].

3.2 Structural, chemical and mechanical properties of the junction zone

The junction zone connects the two valves while the follicle is closed (Fig. 2a-b). During opening, the tissue separates (Fig. 2c-d) and is then exposed to the environment. On the micron level, tooth-like structures with an irregular geometry (Fig. 2e) are visible in all three species after opening. These structures are mostly intact when the valves separate during heat exposure; indicating that heat induced opening seems to cause a rather smooth separation process. In contrast to that, when samples are forced mechanically to separate at room temperature, the surface shows pieces from opposite parts of the junction zone sticking together. Confocal Raman microscopy allows mapping of the waxes in thin cross sections of the tissue (Fig. 3a), and shows that the waxes are predominantly accumulated in between the tooth-like structures (Fig. 3a). These waxes are able to flow in the liquid state, as shown for the boiled section, in which wax droplets are present after heating in water (Fig. 3b-e). Previously, the wax spectra of *B. attenuata* were shown to correlate with cutin features [13, 17], which is not unusual, since cutin is ubiquitous on plant/ fruit surfaces [18], contributing to important cuticle functions, such as prevention of desiccation and organ fusion [19]. Wax spectra obtained from a cluster analysis of image scans (see Fig. S2 for details) show that the wax features are similar for all species, apart from differences in relative band intensity occurring in the spectral region between 1600 – 1700 cm^{-1} (Fig. 4). In this range, vibrational bands of aromatic compounds occur, for example the C=C stretching vibrations of the aromatic ring at 1600 cm^{-1} [20]. In the same region, bands from C=C stretching vibrations of unsaturated fatty acids arise, which appear mainly as conjugated olefinic bonds in *B. attenuata* (band at ~1630 cm^{-1}), whereas in *B. serrata*, a clear additional band from isolated *cis* isomers is present at ~1650 cm^{-1} [21]. This observed discrepancy could explain the small differences in their experimentally determined melting temperature (Fig. 1b and Fig. S1). In *B. candolleana*, a broad band with shoulders appears in the region around 1600 – 1650 cm^{-1}. A higher background, which is probably caused by phenolic compounds (band around 1600 cm^{-1}), and less pronounced bands assigned to unsaturated C=C bands (1630 and 1650 cm^{-1}) suggest a different aromatic and wax composition in this species.

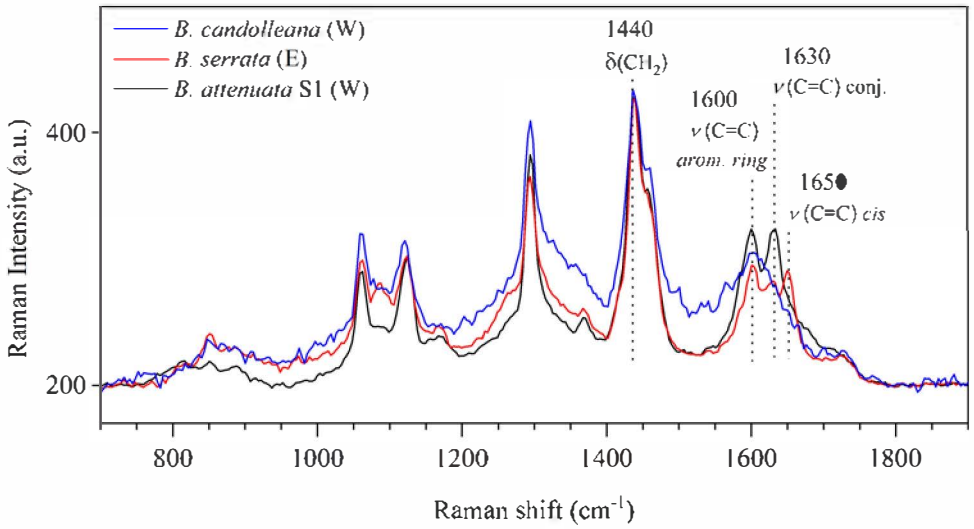

Figure 4. Wax spectra identified in the junction zone of different *Banksia* species. Spectral region from 750-1900 cm^{-1} shown for Western (W) and Eastern (E) species after performing a cluster analysis of image scans. All spectra are normalized to the peak at 1440 cm^{-1}. *B. attenuata* originates from collection site 1. Peak assignments are based on Larkin [21]; the regions/ image scans used for clustering are shown in Fig. S2 (Supplementary Materials).

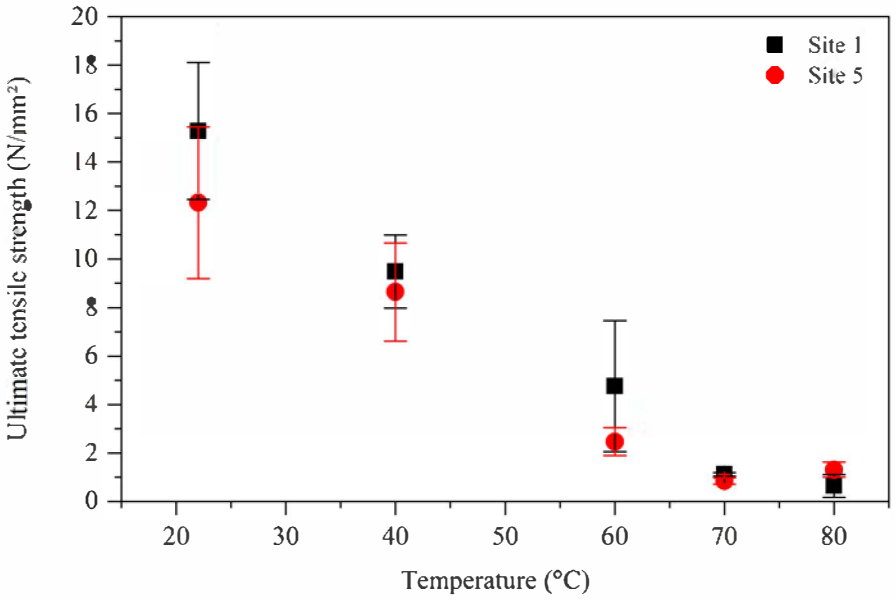

Figure 5. Ultimate tensile strength of the junction zone in *B. attenuata* at different temperatures. Experimental data for samples from the two extreme sites (Follicle opening temperatures: Site 5: To,50%=54°C; Site 1: To, 50%=72°C). Data points represent means ± SD for all samples. High error bars at lower temperatures could be a result of varying moisture contents in the samples, sample geometry or the position from which the sample was cut out for testing (the pulling angle in the follicle might be different).

In general, phenolic compounds are common in cuticles [18] and have been shown to play an important role in land plant evolution [22]. Their concentration was found to vary depending on the developmental stage of fruits [23]. General parameters that affect the phase transition temperatures of lipids are the hydrocarbon length, degree of unsaturation and bond configuration (packing of C=C *trans* chains is easier than C=C *cis* due to steric hindrance), charge, nature of the head group and mixing ratio, if different lipids or other compounds are present.

Mechanical testing of the junction zone in *B. attenuata* follicles from site 1 (high opening temperature) and site 5 (lower opening temperature) shows that the ultimate tensile strength strongly decreases as temperature increases up to 60-70 °C (Fig. 5). This decrease occurs continuously and simultaneously for samples from both sites. At temperatures higher than 70 °C, the tensile strength remains at a constant value of less than 2 N mm^{-2}. A similar temperature induced decrease in the ultimate tensile strength has been described for paraffin wax below its melting temperature [24]. Considering these observations, follicle opening appears to be facilitated at elevated temperatures by requiring less force for valve separation. However, due to the mismatch of the opening and melting temperatures (the wax is already liquid around 50-55 °C) along with the mechanical behaviour of the junction zone, melting is not sufficient for follicle opening. Instead, our research has recently linked the mechanism for opening to a decrease in the elastic modulus of the follicle endocarp at high temperatures, which allows releasing of the stresses that have been generated by differential shrinkage of the tissue during maturation and drying [13]. The same study shows that differences in the opening temperatures can be explained by variations in follicle geometry. Based on these results and the findings from the present study, temperature appears to trigger multiple processes relevant for opening by affecting the elastic properties of the endocarp, but also the ultimate tensile strength of the junction zone.

3.3 The self-sealing mechanism

Wax melting in the junction zone does not coincide with follicle opening. Therefore, the waxes are likely to serve a different function in the system, which, we suggest, is follicle (self-) sealing. We attribute this function to the waxes on the basis of their distinct physicochemical properties and the climatic conditions in the natural distribution range of the plants. For the samples collected in the field (*B. attenuata* and *B. candolleana*) it is known that the air temperature required for melting and damage repair in the sealing layer can be reached on a hot summer day [4]. In order to support the hypothesis of a self-sealing function

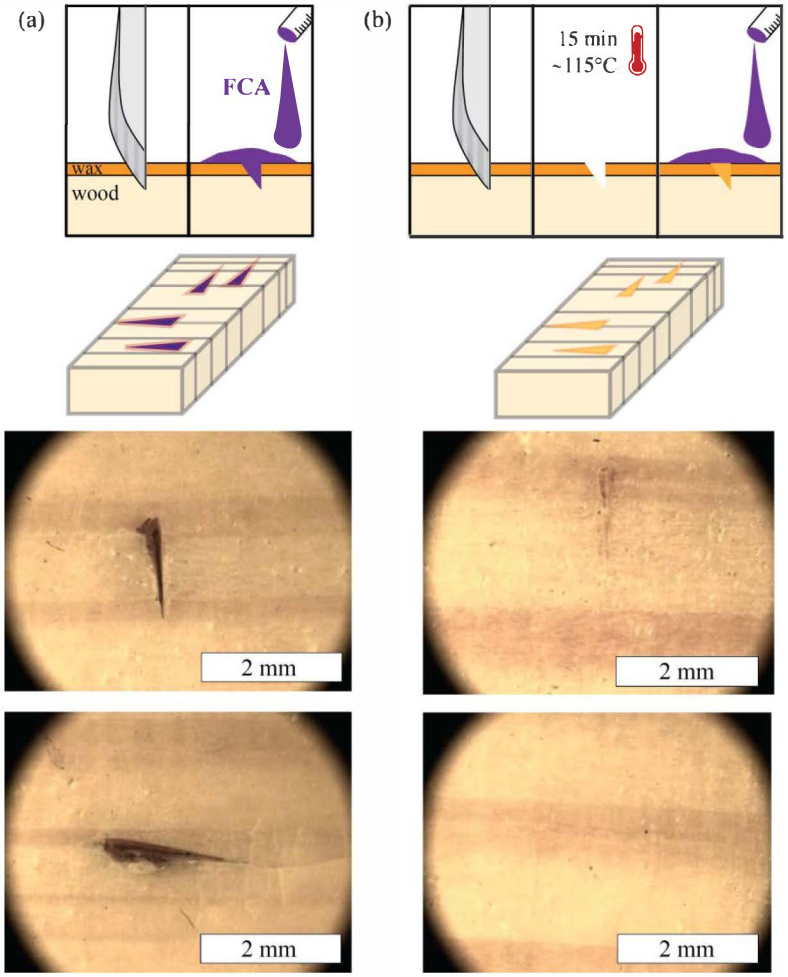

Figure 6. *Banksia* inspired self-sealing system composed of Carnauba wax sealed wood platelets. Schematic representation of the procedures and microscopic view of the cuts (perpendicular and parallel to the fiber direction) after FCA staining. (a) Non-heated samples and (b) heated samples showing sealed cuts and lack of staining.

for the waxes, developmental changes in the follicles and their effects on the follicle structure need to be taken into account. Initially, during follicle development and maturation, the tissue is hydrated and alive [14]. Whilst it is not known at which stage cell death occurs and the water supply to follicles is terminated, these processes promote drying of the follicle, leading to stress development in the two hygroscopic valves by differential shrinkage due to the orientation and structure of the valve tissue [14]. Furthermore, daily fluctuations in follicle moisture content can be observed depending on the environmental conditions. Therefore, we assume that small dimensional changes take place during canopy storage of the follicles, which might lead to the formation of micro-cracks in the junction zone. At temperatures below the actual opening temperature (at 50-55 °C), the waxes are liquid and are thereby able to seal cracks in the confined volume between the two valves on hot days. The flow of the liquid is facilitated by the volumetric expansion and a reduction in viscosity, two distinctive features of the melting process in waxes [25]. Based on this mechanism, every melting event, during which the necessary temperature for opening is not reached, will result in re-sealing of the closed follicles. In this way, the melting enables an effective restoration of the barrier properties. During the rainy season, minimising diffusion of water into the closed follicle is important for maintaining a low moisture content to prevent germination of the seeds, to enhance seed longevity, and to prohibit growth of fungi or other microbes. During the dry season, on the other hand, water diffusion out of the follicle needs to be limited to reduce dimensional changes in the valves, which will influence opening properties.

3.4 The model system confirms self-sealing induced by wax melting

In order to test whether heating allows efficient sealing of micro-cracks, a model system based on pine wood impregnated with a layer of Carnauba wax was used (Fig. 6). Heating ($T > T_m$) of the samples sealed cuts in the impregnated wood effectively after 15 min. None of the heat treated cuts parallel to the fibre direction showed positive FCA staining and only 6 % of the perpendicular cuts stained positive, showing that the staining solution could mostly not penetrate into the wood through the cuts. On the reference samples, which did not experience heating, 100 % of the parallel cuts stained, and 81 % of the cuts perpendicular to the fibre direction showed positive staining. Therefore, heating significantly reduced or prevented the penetration of the staining solution into the wood by re-establishing the wax barrier at the fibre-atmosphere interface, which confirms the self-sealing capability in a simplified, mimicked system.

3.5 Conclusions

The embedment of an agent which melts at slightly elevated temperatures to fill voids and cracks and re-solidifies afterwards, is known in engineering as a typical system for self-healing [26, 27]. However, it requires a temperature stimulus to initiate the process, and is therefore not always desirable in technical applications, since autonomously running mechanisms are often preferred [28]. Nevertheless, in a specific operational environment, where conditions change naturally and stimuli are provided frequently, the sealing system could be mimicked and applied. The process is repeatable due to its temperature dependence and lack of consecutive structural inactivation, e.g. lack of (irreversible) cross-linking of the wax.

The underlying principles of the described self-sealing mechanism, namely a phase transition concomitant with volumetric expansion and a reduction in fluid viscosity of the sealing agent, could be used as a basis for system modifications, e.g. for the design of pressure or pH/chemically sensitive compartments as self-sealing agents in smart materials. A modified system based on the principles of (pressure driven) volume expansion and (chemically induced) phase transition has only recently been discovered in other plant taxa [29], and has already reached the stage of technical implementation in the shape of solvent filled microcapsule embedment [26, 30, 31].

In an ecological context, the waxes in the junction zone of the follicles are likely to play an important role in regulating gas and water exchange between the valve tissue and the surrounding atmosphere. Self-sealing is beneficial for regulating seed moisture content and for preventing microbial penetration and growth over long time periods. Based on the specific properties of the waxes identified in three selected species, we suggest that such a self-sealing mechanism is essential for maintaining dimensional stability of the valves, but also for maximising seed viability during storage inside the follicles and within the plant canopy.

Data accessibility

All raw data and sample materials are stored at the MPIKG and are accessible upon request.

Authors' contributions

M.E., D.J.M., B.P.M. and P.F. conceptualized the project. J.C.H. and D.J.M. collected samples and performed opening experiments. J.C.H., O.S., N.G. and M.E. designed and performed the other experiments. J.C.H., N.G., O.S., M.E. and P.F. analysed and interpreted

data. J.C.H. wrote the manuscript draft; O.S., M.E., D.J.M., B.P.M., C.N. and P.F. reviewed the manuscript and approved publication.

Competing interests

The authors declare no competing interests.

Acknowledgements

The authors thank Kevin Collins for providing *Banksia* cones from his farm in Western Australia and for sharing his valuable insights. The Botanic Garden in Bonn is acknowledged for providing further sample material. All authors thank the Max Planck Society and the European Cooperation in Science and Technology (COST Action FP1105) for funding. JCH acknowledges the support in the field by Sebastian Ehrig, and NG acknowledges funding from the Austrian Science foundation (FWF, Y728-B16) and European Research Council (ERC, grant agreement No. 681885).

References

[1] Meyers, M.A., McKittrick, J. & Chen, P.Y. 2013 Structural Biological Materials: Critical Mechanics-Materials Connections. *Science* **339**, 773-779. (doi:10.1126/science.1220854).
[2] Bauer, G., Nellesen, A. & Speck, T. 2010 Biological lattices in fast self-repair mechanisms in plants and the development of bio-inspired self-healing polymers. *Wit Trans Ecol Envir* **138**, 453-459. (doi:10.2495/Dn100401).
[3] Konrad, W., Flues, F., Schmich, F., Speck, T. & Speck, O. 2013 An analytic model of the self-sealing mechanism of the succulent plant Delosperma cooperi. *J Theor Biol* **336**, 96-109. (doi:10.1016/j.jtbi.2013.07.013).
[4] Cowling, R.M. & Lamont, B.B. 1985 Variation in Serotiny of 3 Banksia Species Along a Climatic Gradient. *Aust J Ecol* **10**, 345-350. (doi:10.1111/j.1442-9993.1985.tb00895.x).
[5] Whelan, R.J., De Jong, N.H. & Von der Burg, S. 1998 Variation in bradyspory and seedling recruitment without fire among populations of Banksia serrata (Proteaceae). *Aust J Ecol* **23**, 121-128. (doi:10.1111/j.1442-9993.1998.tb00710.x).
[6] Collins, K., Collins, K. & George, A.S. 2009 *Banksias*. 1st ed. ed. Melbourne, Vic., Bloomings Books.
[7] Enright, N.J. & Lamont, B.B. 1989 Fire Temperatures and Follicle-Opening Requirements in 10 Banksia Species. *Aust J Ecol* **14**, 107-113.
[8] Lamont, B.B., Lemaitre, D.C., Cowling, R.M. & Enright, N.J. 1991 Canopy Seed Storage in Woody-Plants. *Bot Rev* **57**, 277-317. (doi:10.1007/Bf02858770).
[9] Bradstock, R.A., Bedward, M., Scott, J. & Keith, D.A. 1996 Simulation of the effect of spatial and temporal variation in fire regimes on the population viability of a Banksia species. *Conserv Biol* **10**, 776-784. (doi:10.1046/j.1523-1739.1996.10030776.x).
[10] Bell, D.T. 2001 Ecological response syndromes in the flora of southwestern Western Australia: Fire resprouters versus reseeders. *Bot Rev* **67**, 417-440. (doi:10.1007/Bf02857891).
[11] Lamont, B.B. & Markey, A. 1995 Biogeography of Fire-Killed and Resprouting Banksia Species in South-Western Australia. *Aust J Bot* **43**, 283-303. (doi:10.1071/Bt9950283).
[12] Bradstock, R.A., Gill, A.M., Williams, R.J. & CSIRO. 2012 *Flammable Australia : fire regimes, biodiversity and ecosystems in a changing world*. Collingwood, Vic., CSIRO Publishing; x, 333 p. p.

[13] Huss, J.C., Schoeppler, V., Merritt, D.J., Best, C., Maire, E., Adrien, J., Spaeker, O., Janssen, N., Gladisch, J., Gierlinger, N., et al. 2018 Climate-Dependent Heat-Triggered Opening Mechanism of Banksia Seed Pods. *Advanced Science* **5**. (doi:10.1002/advs.201700572).
[14] Wardrop, A.B. 1983 The Opening Mechanism of Follicles of Some Species of Banksia. *Aust J Bot* **31**, 485-500. (doi:10.1071/Bt9830485).
[15] Lewis, R.N.A.H. & McElhaney, R.N. 2006 Vibrational Spectroscopy of Lipids. In *Handbook of Vibrational Spectroscopy* (John Wiley & Sons, Ltd.
[16] Mulisch, M. & Welsch, U. 2010 *Romeis Mikroskopische Technik*, Springer Spektrum.
[17] Mateu, B.P., Hauser, M.T., Heredia, A. & Gierlinger, N. 2016 Waterproofing in Arabidopsis: Following Phenolics and Lipids In situ by Confocal Raman Microscopy. *Front Chem* **4**. (doi:10.3389/fchem.2016.00010).
[18] Dominguez, E., Heredia-Guerrero, J.A. & Heredia, A. 2011 The biophysical design of plant cuticles: an overview. *New Phytol* **189**, 938-949. (doi:10.1111/j.1469-8137.2010.03553.x).
[19] Weng, H., Molina, I., Shockey, J. & Browse, J. 2010 Organ fusion and defective cuticle function in a lacs1 lacs2 double mutant of Arabidopsis. *Planta* **231**, 1089-1100. (doi:10.1007/s00425-010-1110-4).
[20] Edwards, H.G.M. & Falk, M.J.P. 1997 Fourier-transform Raman spectroscopic study of unsaturated and saturated waxes. *Spectrochim Acta A* **53**, 2685-2694. (doi:10.1016/S1386-1425(97)00161-3).
[21] Larkin, P. 2011 *Infrared and raman spectroscopy : principles and spectral interpretation.* Amsterdam ; Boston, Elsevier; 73-115 p.
[22] Renault, H., Alber, A., Horst, N.A., Lopes, A.B., Fich, E.A., Kriegshauser, L., Wiedemann, G., Ullmann, P., Herrgott, L., Erhardt, M., et al. 2017 A phenol-enriched cuticle is ancestral to lignin evolution in land plants. *Nat Commun* **8**. (doi:10.1038/ncomms14713).
[23] Dominguez, E., Cuartero, J. & Heredia, A. 2011 An overview on plant cuticle biomechanics. *Plant Sci* **181**, 77-84. (doi:10.1016/j.plantsci.2011.04.016).
[24] Seyer, W.F. & Inouye, K. 1935 Paraffin wax - Tensile strength and density at various temperatures. *Ind Eng Chem* **27**, 567-570. (doi:10.1021/ie50305a016).
[25] Katakura, N. 1980 Viscoelastic behaviour of inlay waxes (part 1). Physical and dynamic viscoelastic properties of several raw material waxes (author's transl). *Shika rikogaku zasshi. Journal of the Japan Society for Dental Apparatus and Materials* **21**, 209-216.
[26] Blaiszik, B.J., Kramer, S.L.B., Olugebefola, S.C., Moore, J.S., Sottos, N.R. & White, S.R. 2010 Self-Healing Polymers and Composites. *Annual Review of Materials Research* **40**, 179-211. (doi:10.1146/annurev-matsci-070909-104532).
[27] Nosonovsky, M. & Rohatgi, P.K. 2012 Biomimetics in Materials Science: Self-healing, Self-Lubricating, and Self-Cleaning Materials. *Springer Ser Mater S* **152**, 1-415. (doi:10.1007/978-1-4614-0926-7).
[28] Urban, M.W. 2009 Stratification, stimuli-responsiveness, self-healing, and signaling in polymer networks. *Prog Polym Sci* **34**, 679-687. (doi:10.1016/j.progpolymsci.2009.03.004).
[29] Speck, T., Mulhaupt, R. & Speck, O. 2013 Self-Healing in Plants as Bio-Inspiration for Self-Repairing Polymers. *Self-Healing Polymers: From Principles to Applications*, 61-89. (doi:Book_Doi 10.1002/9783527670185).
[30] Jin, H.H., Mangun, C.L., Stradley, D.S., Moore, J.S., Sottos, N.R. & White, S.R. 2012 Self-healing thermoset using encapsulated epoxy-amine healing chemistry. *Polymer* **53**, 581-587. (doi:10.1016/j.polymer.2011.12.005).
[31] Jones, A.R., Watkins, C.A., White, S.R. & Sottos, N.R. 2015 Self-healing thermoplastic-toughened epoxy. *Polymer* **74**, 254-261. (doi:10.1016/j.polymer.2015.07.028).

Temperature-induced self-sealing capability of *Banksia* follicles

J.C. Huss, O. Späker, N. Gierlinger, D.J. Merritt,
B.P. Miller, C. Neinhuis, P. Fratzl, M. Eder

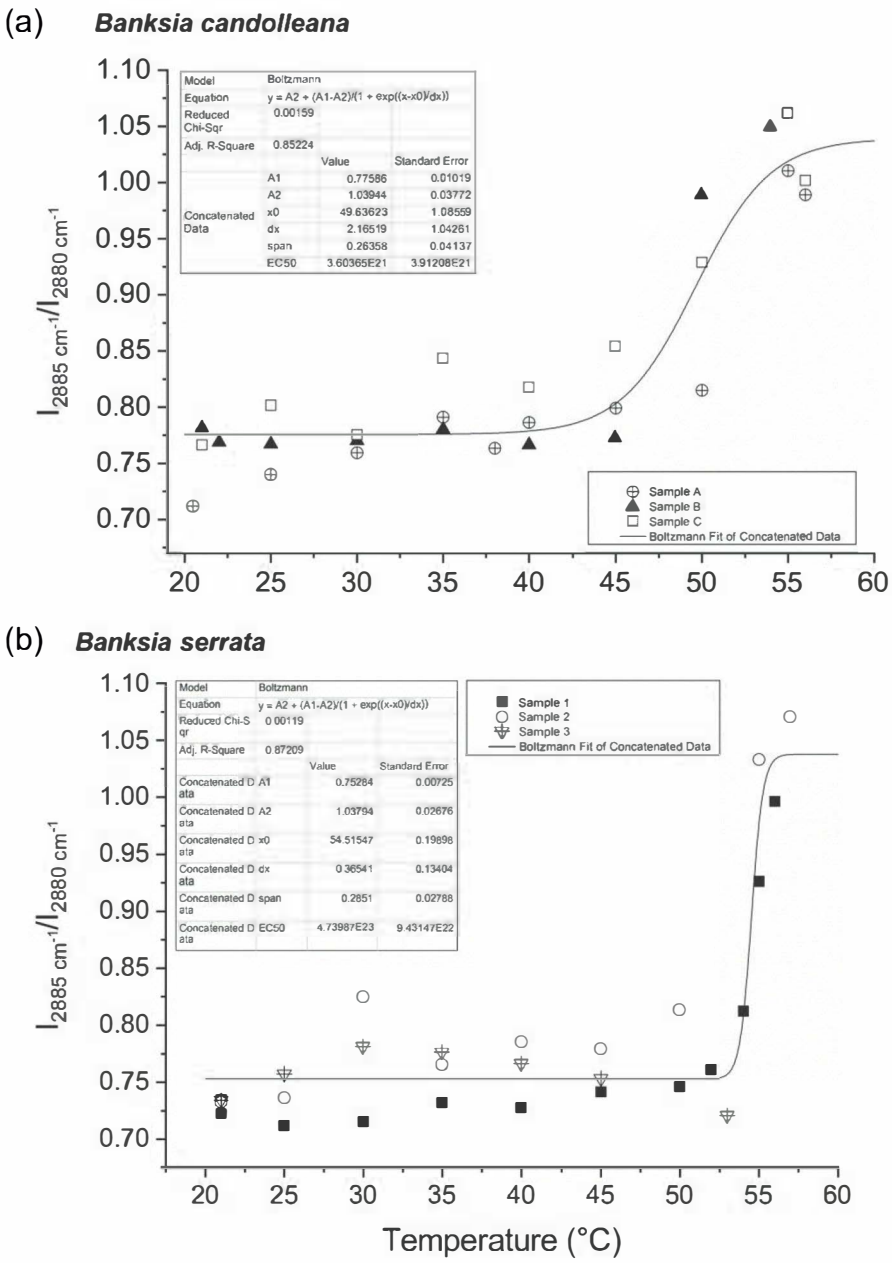

Figure S1. Determined wax melting temperatures for *B. candolleana* (a) and *B. serrata* (b) based on *in situ* Raman measurements of the waxes in the junction zone. Intensity ratios of the two selected bands change upon heating, indicating wax melting around the inflection point of the fitted curve.

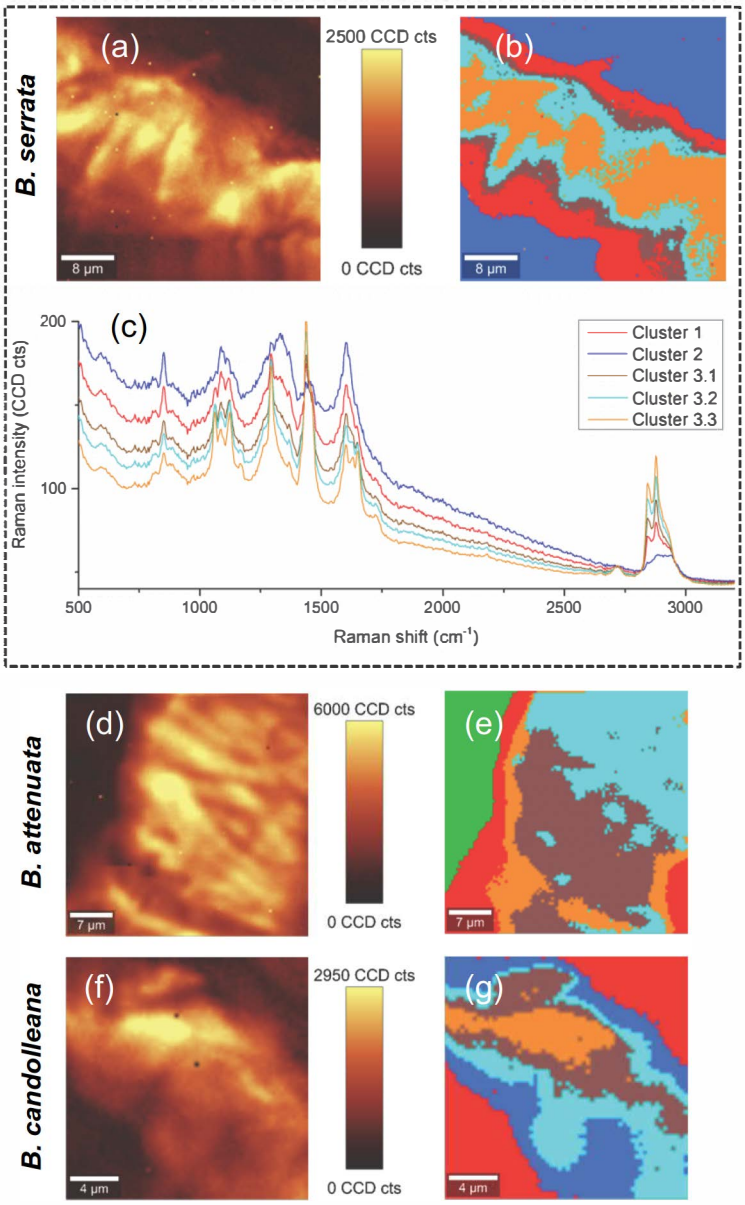

Figure S2. Cluster analysis for *B. serrata, B. attenuata* and *B.candolleana*. Images (a),(d),(f) were created by integration of the spectral region from 2810-2990 cm^{-1} and give an overview of the wax distribution and signal intensity in each sample. The coloured images (b),(e),(g) show the individual clusters obtained from the analysis, each cluster is represented by a different colour (5 in total). The spectra in (c) correspond to the clusters in (b) and illustrate the spectral changes (composition and background) across the junction zone in *B. serrata.*

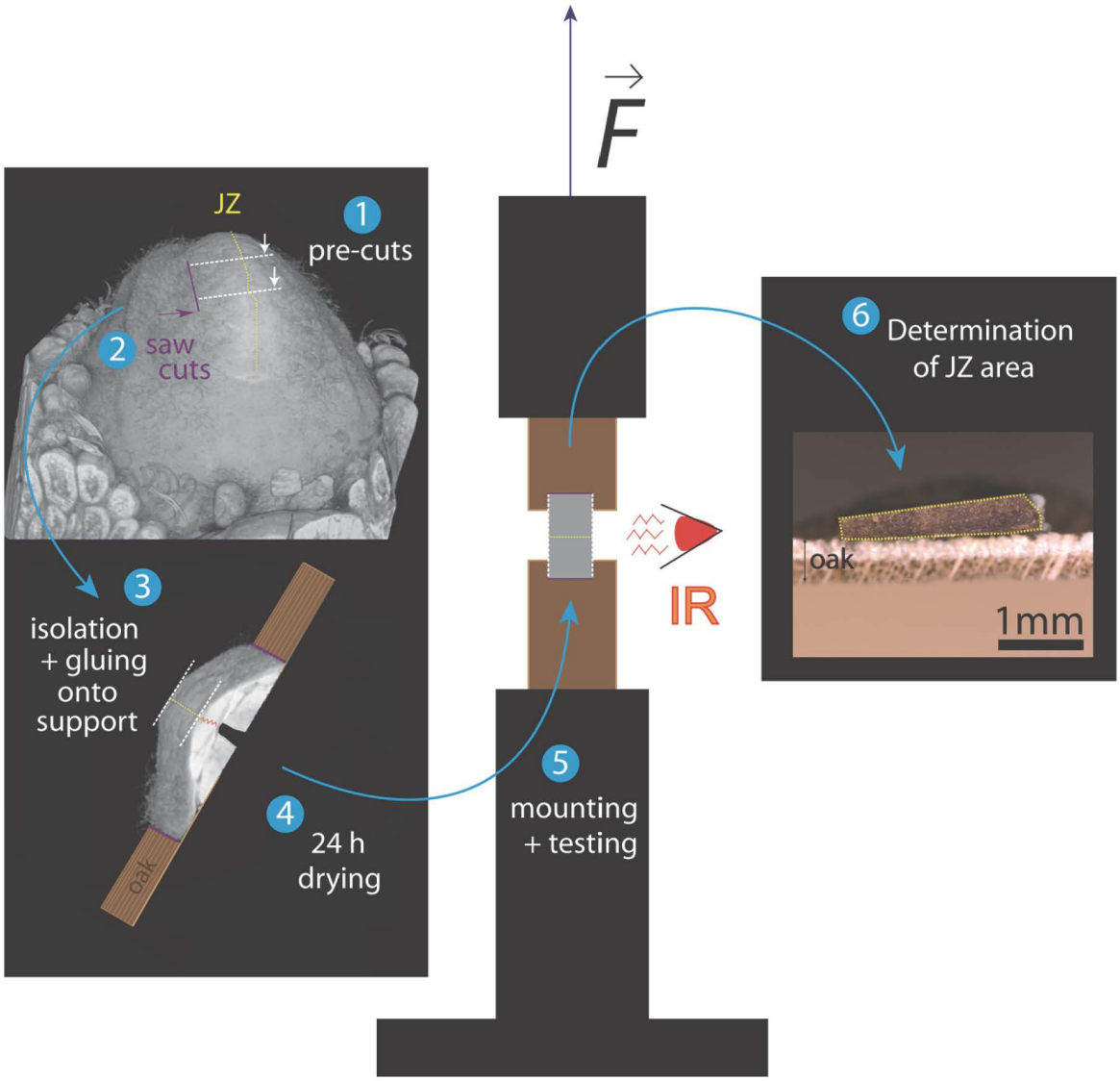

Figure S3. Schematic representation of the tensile testing set-up: After sample isolation (1-3 with cutting planes indicated by arrows), they were glued onto oak support veneers (3) and mouted (5) after drying (4). During testing, the samples were heated with an infrared source (IR) heating the sample that is fixed to holders, which are pulled apart during the experiment. After the experiment, the contact area in the JZ (6) was determined for normalisation of the force. For illustration purposes, dimensions in 1-5 are not to scale (true dimensions shown in 6).